THE JOURNAL OF BIOLOGICAL CHEMISTRY VOL. 282, NO. 29, pp. 21448–21459, July 20, 2007

NMR Investigation of Tyr^{105} Mutants in TEM-1 β-Lactamase

DYNAMICS ARE CORRELATED WITH FUNCTION[*] [S]

Received for publication, October 17, 2006, and in revised form, March 14, 2007 Published, JBC Papers in Press, April 10, 2007, DOI 10.1074/jbc.M609777200

Nicolas Doucet[‡1], **Pierre-Yves Savard**[§1], **Joelle N. Pelletier**[‡¶2], **and Stéphane M. Gagné**[§3]

From the [‡]*Département de Biochimie, Université de Montréal, Montréal, Québec H3C 3J7, the* [§]*Département de Biochimie et de Microbiologie et CREFSIP, Université Laval, Québec, Québec G1K 7P4, and the* [¶]*Département de Chimie, Université de Montréal, Montréal, Québec H3C 3J7, Canada*

The existence of coupled residue motions on various time scales in enzymes is now well accepted, and their detailed characterization has become an essential element in understanding the role of dynamics in catalysis. To this day, a handful of enzyme systems has been shown to rely on essential residue motions for catalysis, but the generality of such phenomena remains to be elucidated. Using NMR spectroscopy, we investigated the electronic and dynamic effects of several mutations at position 105 in TEM-1 β-lactamase, an enzyme responsible for antibiotic resistance. Even in absence of substrate, our results show that the number and magnitude of short and long range effects on ^{1}H-^{15}N chemical shifts are correlated with the catalytic efficiencies of the various Y105*X* mutants investigated. In addition, ^{15}N relaxation experiments on mutant Y105D show that several active-site residues of TEM-1 display significantly altered motions on both picosecond-nanosecond and microsecond-millisecond time scales despite many being far away from the site of mutation. The altered motions among various active-site residues in mutant Y105D may account for the observed decrease in catalytic efficiency, therefore suggesting that short and long range residue motions could play an important catalytic role in TEM-1 β-lactamase. These results support previous observations suggesting that internal motions play a role in promoting protein function.

Enzymes are extremely efficient catalysts that can accelerate biochemical reactions up to a factor of 10^{18} when compared with the same uncatalyzed reaction (1). Although considerable progress has been made in understanding enzyme catalysis over the past few years (2, 3), the detailed explanation of this large rate enhancement remains a significant challenge. Historically regarded as relatively static entities, increasing evidence now suggests that enzymes behave as dynamic machines and that motions on various time scales play important roles in promoting enzyme catalysis (4). To this day, only a small number of enzymes have been shown to rely on essential proximal and/or distal coupled residue motions for catalysis, among which dihydrofolate reductase (5–8), cyclophilin A (9, 10), liver alcohol dehydrogenase (11–14), triose-phosphate isomerase (15–19), and ribonuclease A (20–22) remain some of the best characterized systems (for recent reviews see Refs. 23 and 24). Analogous behavior among other enzymes remains to be elucidated, although the confirmation of such phenomena in structurally and functionally unrelated protein families and folds suggests that this may be a widespread process (24). A general view of such correlation between structure, function, and dynamics in enzymes would greatly improve our current understanding of these powerful catalysts. In this study, we provide experimental evidence supporting the importance of active-site residue motions in the enzyme TEM-1 β-lactamase through the characterization of various Y105*X* mutants by NMR spectroscopy.

We have previously investigated the role of the active-site residue Tyr^{105} in TEM-1 β-lactamase using saturation mutagenesis, enzyme kinetics, and *in silico* molecular dynamics studies (25). Our results show that this residue is mainly involved in substrate discrimination and stabilization at the active site of TEM-1. Aromatic residues at position 105 were shown to play an important role in substrate stabilization by preventing steric hindrance with substrate molecules through the formation of a rigid, stabilizing wall that restricts the active-site cavity size, and therefore substrate movement. Most non-aromatic residue replacements at position 105 were found to possess too many degrees of freedom for appropriate substrate stabilization, thus explaining the strong aromatic bias observed in other class A β-lactamases at this active-site position. Interestingly, Y105G, Y105N, and Y105A were moderately active in hydrolysis of penicillin substrates, despite the fact that they are not aromatic. Increasing side chain length (and flexibility) generally resulted in important decreases in activity. Charged side chains (except the aromatic His) were also poorly compatible with reactivity. These kinetic observations correlated with the extent of Y105*X* side chain motion upon molecular modeling in the presence of a penicillin substrate; only the aromatic and the small residues provided a stable, well organized binding environment over the short time scale tested (picosecond). To further explore dynamics of these TEM-1 β-lactamase active-site mutants, we turned to nuclear magnetic resonance.

* This work was supported by grants from the Natural Sciences and Engineering Research Council of Canada (to J. N. P. and S. M. G.), the Fond Québécois de la Recherche sur la Nature et les Technologies (to J. N. P.), and the Fonds de la Recherche en Santé du Québec (to P. Y. S.). The costs of publication of this article were defrayed in part by the payment of page charges. This article must therefore be hereby marked "*advertisement*" in accordance with 18 U.S.C. Section 1734 solely to indicate this fact.

[S] The on-line version of this article (available at http://www.jbc.org) contains supplemental Fig. S1 and Tables S1–S3.

[1] Both authors contributed equally to this work.

[2] To whom correspondence may be addressed: Dépt. de Chimie, Université de Montréal, C.P. 6128, Succursale Centre-Ville, Montréal, Québec H3C 3J7, Canada. Tel.: 514-343-2124; Fax: 514-343-7586; E-mail: joelle.pelletier@umontreal.ca.

[3] To whom correspondence may be addressed: Dépt. de Biochimie et de Microbiologie et CREFSIP, Université Laval, Québec, Québec G1K 7P4, Canada. Tel.: 418-656-7860; Fax: 418-656-7176; E-mail: stephane.gagne@rsvs.ulaval.ca.

NMR relaxation experiments are powerful techniques that can provide valuable information on the dynamic effects of mutations in the active-site cavity of enzymes during catalysis (10). In addition to providing information on fast dynamics (picosecond-nanosecond (ps-ns)) of protein backbones (26), the time scale of NMR dynamics ranges up to the catalytically relevant microsecond-millisecond (μs-ms) (27). The recent and complete ^{1}H, ^{15}N, ^{13}C backbone resonance assignments of TEM-1 (E28G) β-lactamase by NMR (28) as well as ^{15}N relaxation backbone dynamics studies on the same enzyme (29) now pave the way to the motional characterization of important active-site residues with respect to their effect on catalysis in this enzyme family. To improve the interpretation of our previous molecular modeling and kinetics observations at the molecular level and to verify the proposed motion of residue 105 in TEM-1, this study describes the backbone resonance assignments of TEM-1 mutants Y105D, Y105G, Y105N, and Y105W as well as ^{15}N relaxation and backbone dynamics of wild-type TEM-1 and mutant Y105D. To our surprise, the localized dynamic effects we had originally observed by molecular modeling in the area of position 105 extend to a far broader environment, affecting catalytically relevant motional time scales of important catalytic residues in the active-site cavity of TEM-1. The dynamic investigation of the Y105D mutant and the effects of the Y105*X* mutations on the surrounding environment provide evidence for the importance of active-site residue motions in TEM-1 β-lactamase as well as their possible role in substrate stabilization and catalysis. In addition to long range effects observed for residues distal to the active site as well as evidence offered by previous molecular dynamics investigation performed on a TEM-1 mutant (30), these experimental observations suggest that class A β-lactamases may rely on long range residue motions in substrate recognition as well as for catalysis.

EXPERIMENTAL PROCEDURES

Reagents—Unless otherwise indicated, all chemicals were purchased from Sigma. Bistris propane[4] was purchased from GE Healthcare, and nitrocefin was purchased from Oxoid (Nepean, Ontario, Canada). Restriction and DNA-modifying enzymes were purchased from MBI Fermentas and New England Biolabs. $^{15}NH_4Cl$, [^{13}C]glucose, 2,2-dimethylsilapentane-5-sulfonic acid, and $^{2}H_2O$ were purchased from Cambridge Isotope Laboratories (Andover, MA).

Bacterial Strains and Plasmids—Escherichia coli XL1-Blue (*supE44, hsdR17, recA1, endA1, gyrA46, thi, relA1, lac* F′ [*proAB*$^{+}$, *lacI*^{q}, *lacZ*Δ*M15*, Tn*10*(*tet*^{r})]) was used for cloning and plasmid propagation, whereas *E. coli* BL21(DE3) (*hsdS gal* [λ*c*Its857 *ind*1 *S*am7 *nin*5 *lacUV*5-T7 gene 1]) was used for protein expression. Plasmid pET-TEM-1 (31), in which the wild-type bla_{TEM-1} gene was fused to the leader sequence of *ompA* was a generous gift from Marvin D. Makinen (University of Chicago). It was maintained using 30 μg/ml kanamycin and was used for extracellular protein expression under the control of the T7 promoter in *E. coli* BL21(DE3). The construction of plasmids pQE32Chl-TEM(Y105*X*) containing the Y105*X* mutations of TEM-1 was described elsewhere (25).

Oligonucleotides and Mutagenesis—Oligonucleotide primers used for mutagenesis were synthesized by Integrated DNA Technologies (Coralville, IA) and by the Plate-Forme d'Analyses Biomoléculaires (Université Laval, Québec, Canada). Oligonucleotide primers used for DNA sequencing were synthesized by Li-Cor Biotechnology (Lincoln, NB). The E28G mutation originally present in the pET-TEM-1 construction was reverted back to WT using the QuikChange site-directed mutagenesis kit from Stratagene (La Jolla, CA) with mutagenic primers TEM-G28E-upper (5′-CAGGCCCACCCAGAAACGCTGGTGAAAGTA-3′) and TEM-G28E-lower (5′-TACTTTCACCAGCGTTTCTGGGTGGGCCTG-3′). The Y105D, Y105G, Y105N, and Y105W mutants of TEM-1 (25) were PCR-amplified from vectors pQE32Chl-TEM(Y105*X*) using the two following terminal primers: TEMHinDIIIR (5′-ACACACAAGCTTTTACCAATGCTTAATCAGTGA-3′) and NdeIOmpATEMF (5′-CACACACACATATGAAAAAGACAGCTATCGCGATTGCAGTGGCACTGGCTGGTTTCGCTACCGTAGCGCAGGCCCACCCAGAAACGCTGGTGAAA-3′), a 95-bp forward primer containing both the NdeI restriction site and the *ompA* leader sequence. The resulting recombinant *ompA*-TEM(Y105*X*) genes were sequentially digested with NdeI and PstI and cloned into NdeI/PstI-digested and shrimp alkaline phosphatase-treated pET-TEM-1 before electroporation into *E. coli* XL1-Blue cells. Colonies were individually picked after selection on Luria-Bertani (LB) medium containing 30 μg/ml kanamycin, and the sequence of each mutant was confirmed by the dideoxy chain termination method with the Thermo Sequenase Cycle Sequencing kit from Upstate Biochemical Corp. using dye-labeled primers and a Li-Cor automated sequencer (Lincoln, NB). For protein expression purposes, DNA constructs were transformed into *E. coli* BL21(DE3) cells and sequenced again.

Expression and Purification of ^{15}N-^{13}C-Labeled WT and TEM-1(Y105X) Mutants—Uniformly ^{15}N-^{13}C-labeled TEM-1 samples were prepared using $^{15}NH_4Cl$ and [^{13}C]glucose as the sole nitrogen and carbon sources according to the following protocol. A 2-ml overnight culture of each BL21(DE3)/pET-TEM-1(Y105*X*) clone was used to inoculate 500 ml of M9 minimal medium containing 0.04 M Na_2HPO_4, 0.02 M KH_2PO_4, 0.02 M $^{15}NH_4Cl$, 0.01 M NaCl, 0.3% [^{13}C]glucose, 2 mM $MgSO_4$, 2 μM $FeCl_3$, 0.1 mM $CaCl_2$, 50 μM $ZnSO_4$, 0.5% thiamine, 2.5 mM betaine, and 30 μg/ml kanamycin. The proteins were expressed by propagating the host cells at 37 °C (250 rpm) to an $A_{600\ nm}$ = 0.8 followed by induction with 0.4 mM isopropyl 1-thio-β-D-galactopyranoside and addition of 15 μg/ml kanamycin for 16–18 h at 25 °C (250 rpm). After induction, cells were pelleted by centrifugation (30 min, 10,000 × *g*, 4 °C), and the supernatant was filtered using a 0.45-μm membrane filter prior to a 5-fold concentration using an 8400 stirred cell apparatus from Millipore (Nepean, Ontario, Canada) with an Ultracel Amicon YM-10 membrane (molecular mass cutoff 10,000 Da).

After overnight dialysis at 4 °C against a 10 mM Bistris propane buffer (pH 6.6), purification of WT and TEM(Y105*X*) mutants was performed on an ÄKTAexplorer chromatography

[4] The abbreviations used are: Bistris propane, 1,3-bis[tris(hydroxymethyl)-methylamino]propane; NOE, nuclear Overhauser effect; WT, wild type; PDB, Protein Data Bank; ps-ns, picosecond-nanosecond; μs-ms, microsecond-millisecond; HSQC, heteronuclear single quantum coherence.

system from GE Healthcare as reported previously (29). In all cases, purity was estimated to be higher than 95% by SDS-PAGE, and liquid chromatography/mass spectrometry/electrospray ionization and yields were typically ~50 mg/liter of pure protein for all TEM-1(Y105*X*) mutants.

NMR Samples—For the acquisition of NMR spectra, WT and mutants Y105D, Y105G, Y105N, and Y105W were lyophilized after extensive dialysis against H_2O. The enzymes were subsequently dissolved to a concentration of 0.8 mM in a 90% H_2O, 10% ^2H_2O solution containing 4 mM imidazole and 0.1 mM 2,2-dimethylsilapentane-5-sulfonic acid for internal pH and chemical shift referencing, respectively. All experiments were performed at pH 6.6.

NMR Spectroscopy—All NMR experiments were performed at 30 °C on a Varian INOVA 600 spectrometer operating at a proton frequency of 599.739 MHz equipped with a *z* axis gradient and a triple resonance cryoprobe. Two-dimensional ^1H-^{15}N HSQC, three-dimensional HNCO, three-dimensional HN(CO)CA, and three-dimensional CBCA(CO)NH spectra (Biopack, Varian Inc., Palo Alto, CA) together with assignments obtained for TEM-1 E28G (28) were used to determine sequence-specific assignments for the polypeptide backbone of WT and mutant Y105W. Other mutants (Y105D, Y105G, and Y105N) were assigned by comparison using a combination of two-dimensional ^1H-^{15}N HSQC and three-dimensional HNCO spectra.

^{15}N relaxation experiments were performed on WT and on the Y105D mutant using ^{15}N-^{13}C double-labeled samples for all experiments. ^{15}N-T_1 experiments were performed using sensitivity-enhanced inversion-recovery pulse sequence with pulsed field gradients developed by Kay and co-workers (32). ^{15}N-T_2 experiments were performed using the BioPack pulse sequence from Varian, Inc. (Palo Alto, CA) (33). An *RF* field strength of 6.579 kHz was used for the ^{15}N 180° pulses in the CPMG sequence with an inter-pulse delay of 587 μs. Delay times were 10.9, 21.7, 43.5, 87.0, 173.9, 347.8, 695.7, 1391.3, and 1989.1 ms for T_1 and 10, 30, 50, 70, 90, 110, 130, 150, and 190 ms for T_2. $\{^1H\}$-^{15}N steady state NOEs were obtained by acquiring spectra with and without ^1H saturation applied before the start of the experiments using a pulse sequence obtained from Kay and co-workers (32). A saturation time of 4 s was used for $\{^1H\}$-^{15}N NOE experiments. To eliminate the potential effect of sample or field homogeneity degradation over time on measured exponential decays, relaxation delays were acquired in an interleaved manner. For example, the acquisition order for the ^{15}N-T_2 relaxation experiments was 10, 50, 90, 130, 30, 70, 110, 150, and 190 ms (34, 35).

Data Analysis—All NMR data were processed with NMRPipe/NMRDraw (36) and analyzed with NMRView (37). For relaxation experiments, ^1H-^{15}N spectra were processed using either a 90° or a 60° shifted sine apodization function in *F*2 (^1H) and either a 90° or a 60° shifted sine-squared function in *F*1 (^{15}N). The 90° processing was used for the great majority of residues, and the 60° processing allowed the separation of a few peaks exhibiting slight overlapping. Linear prediction was performed in *F*1 to extend the time domain by a factor of 1.5, and both dimensions were zero-filled to the next power of 2. For each ^{15}N-T_1 and ^{15}N-T_2 experiment, the spectrum with the shortest relaxation delay (highest intensities) was peak-picked with NMRView, and each ellipse was manually adjusted to fit the peak. The same procedure was used for $\{^1H\}$-^{15}N NOE spectra.

The ^{15}N R_1 and R_2 relaxation rates were determined by fitting T_1 and T_2 curves to a two-parameter exponential decay of the form shown in Equation 1,

$$V(t) = V_0 e^{(-Rt)} \quad \text{(Eq. 1)}$$

where $V(t)$ is the volume after a delay time t; V_0 is the volume at time $t = 0$; and R is either $R_1 = 1/T_1$ or $R_2 = 1/T_2$. Fitting was accomplished using the program CURVEFIT (AG Palmer, Columbia University). R_1 and R_2 uncertainties were calculated using Jackknife simulations (63), and for each data set the minimum error used for further calculation was set to the mean error. $\{^1H\}$-^{15}N NOE values were obtained from the ratio of the volumes of experiments recorded with and without proton saturation. The uncertainties on the $\{^1H\}$-^{15}N NOE values were obtained using the method described by Nicholson *et al.* (38).

Model-free—The internal motion parameters were optimized for the relaxation data according to the model-free formalism pioneered by Lipari and Szabo (39, 40) and extended by Clore *et al.* (41, 42) using the program ModelFree 4.16 (AG Palmer, Columbia University) and the statistical approach of Mandel *et al.* (43). An axially symmetric diffusion model was used in our analysis. Initial estimates of the global tumbling parameters were obtained using the program QUADRIC (AG Palmer, Columbia University). Residues with $\{^1H\}$-^{15}N NOE <0.65 were not considered, and neither were residues with high R_2 ($R_2 \geq \langle R_2 \rangle + \sigma_{R2}$), unless their corresponding R_1 values were low ($R_1 \leq \langle R_1 \rangle - \sigma_{R1}$) (44). The value used for ^{15}N chemical shift anisotropy was −172 ppm and the N–H bond length was set to 1.02 Å. For each simulation, 500 randomly distributed data sets were generated, and discrimination between models was performed using *F*-statistics analysis.

The five models used to describe the spin-relaxation data were as follows: model 1, S^2; model 2; S^2, τ_e; model 3, S^2, R_{ex}; model 4, S^2, τ_e, R_{ex}; and model 5, S^2, τ_e, S^2_f, where S^2 is the order parameter used to characterize the amplitude of the internal motions on the ps-ns time scale. S^2 is a measure of the degree of spatial restriction of the ^1H-^{15}N bond vector and has values ranging from 0, indicating unrestricted motions, to 1, for completely restricted motions; S^2_f is the order parameter for fast motions; τ_e is the effective correlation time for internal motions; and R_{ex} is an exchange term to account for contributions to R_2 from μs-ms time scale motions.

Estimation of the Tyr^{105} Ring Current Effects and Prediction of Chemical Shift Changes Induced by the Mutation—Ring current effects of the Tyr^{105} aromatic group on the chemical shifts of other residues were estimated using the program SHIFTS (version 4.1.1) (45) for TEM-1 with Tyr^{105} positioned in two alternate conformations (positions A and B). Position A places Tyr^{105} as observed in the free-enzyme conformation of TEM-1 (Protein Data Bank, Brookhaven National Laboratory; PDB coordinates 1BTL) (46), whereas position B places Tyr^{105} as observed in the imipenem-bound flipped conformation (PDB coordinates 1BT5) (47). Minimized PDB files were created using the InsightII package, version 2000.1 (Accelrys, San Diego, CA) according to the following protocol. For position A,

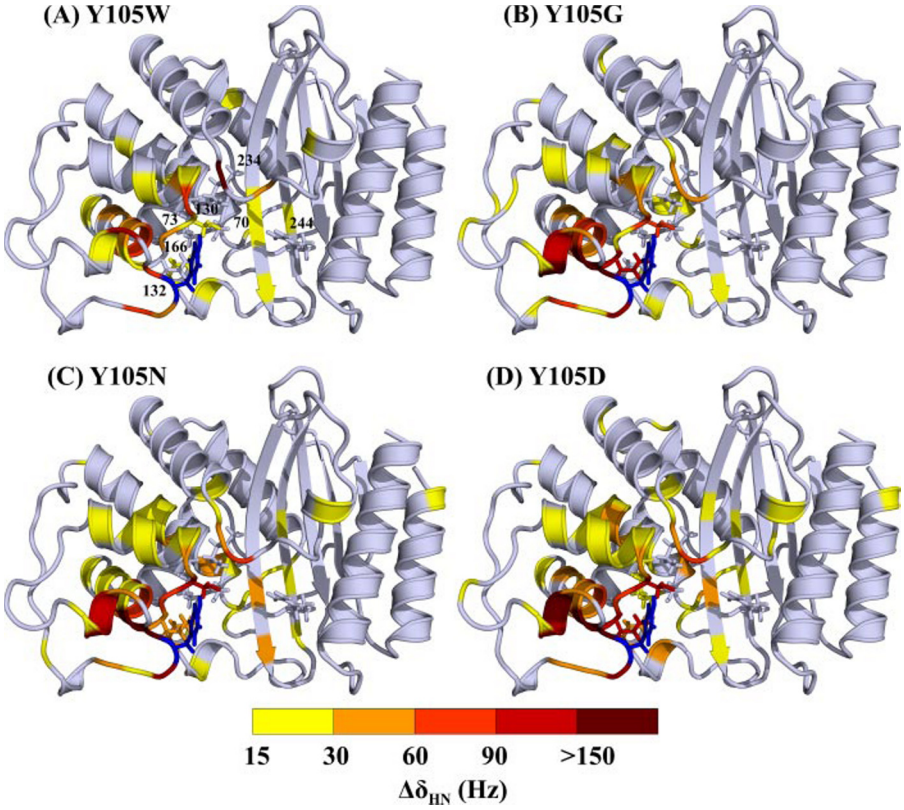

FIGURE 1. **Structural mapping of ^{1}H-^{15}N backbone chemical shift differences ($\Delta\delta_{HN}$) (Hz) calculated between wild-type TEM-1 and mutants Y105W (*A*), Y105G (*B*), Y105N (*C*), and Y105D (*D*).** Values were obtained from two-dimensional ^{1}H-^{15}N HSQC spectra by calculating the differences in peak positions for all assigned residues of the enzyme ($\Delta\delta_{HN} = \sqrt{\Delta\delta_H^2 + \Delta\delta_N^2}$). The *yellow* to *dark-red* gradient displays $\Delta\delta_{HN}$ from 15 to >150 Hz, and unassigned residues and $\Delta\delta_{HN}$ <15 Hz (not significant) are colored *gray*. Catalytic residues Ser^{70}, Lys^{73}, Ser^{130}, Asn^{132}, Glu^{166}, Lys^{234}, and Arg^{244} are labeled and displayed as *stick* representation. Tyr^{105} is colored *blue* and displayed as *stick* representation.

the 1.8-Å crystallographic structure of the *E. coli* TEM-1 β-lactamase (PDB coordinates 1BTL) was used as starting coordinates. The crystallographic water molecules and the active-site SO_4 molecule were deleted, and hydrogen atoms were added at the normal ionization state of the amino acids at pH 7.0. The structure was energy-minimized by applying 1000 steps of steepest descent followed by a conjugate gradient minimization until convergence of 0.001 kcal mol^{-1} Å^{-1}. For position B, backbone atoms of 1BTL and 1BT5 were superimposed, and the Tyr^{105} side chain of 1BTL was repositioned according to Tyr^{105} in 1BT5 by applying χ1 and χ2 angle torsions. The structure was then minimized using the same protocol as for position A. The contribution of Tyr^{105} to ring current shifts was estimated with all aromatic residues mutated to Ala, except for Tyr^{105}. SHIFTS was also used to predict the effect of the mutation on chemical shifts of other residues of the protein. Observed chemical shift changes were considered meaningful when they were significantly greater than the predicted ones.

Sequence Numbering—Because of technical requirements in NMR analysis, sequence numbering used for TEM-1 and mutants Y105*X* is different from the classical nomenclature proposed by Ambler *et al.* (48). Although sequence numbering starts at 26 to give the active-site serine residue the number 70, residues 239 and 253 are not skipped, and the numbering is sequential from 26 to 288. To avoid any confusion in catalytic and structural interpretation, both nomenclatures are appropriately labeled.

RESULTS

^{15}N-^{13}C-Labeled proteins corresponding to mutants Y105D, Y105G, Y105N, and Y105W of TEM-1 β-lactamase were expressed and purified to homogeneity. These mutants were chosen based on the following structural and functional considerations: Trp because of its aromatic similarity with the native Tyr, the native-like activity of mutant Y105W toward penicillins and cephalosporins, and also because of its frequent occurrence in other class A β-lactamases; Asn because its side chain is much smaller than the native, aromatic Tyr although still being a highly active mutant also occasionally represented in other class A β-lactamases; Gly because, like Ala, it exhibits discrimination with respect to penicillins (high catalytic efficiency) and cephalosporins (low catalytic efficiency); and Asp as a representative of a low activity mutant despite its structural similarity with the highly active Asn mutant (25).

Chemical Shift Differences—Although our previous NMR studies of TEM-1 were carried on the E28G mutant (28, 29), this study was performed without this mutation, and assignments of WT TEM-1 were used (Biological Magnetic Resonance Data Bank accession number 6357). A combination of two-dimensional ^{1}H-^{15}N HSQC, three-dimensional HNCO, three-dimensional HN(CO)CA, and three-dimensional CBCA(CO)NH spectra (Biopack, Varian Inc., Palo Alto, CA) were used to sequentially assign nearly all the backbone ^{1}H, ^{15}N, and ^{13}C′ atoms (BMRB numbers for Y105W, Y105G, Y105N, and Y105D are 7236, 7237, 7238, and 7239, respectively). More than 99% of backbone ^{1}H, ^{15}N, and ^{13}C′ assignments were obtained for non-proline residues of each enzyme tested. For WT and mutants Y105D, Y105G, and Y105N, the missing assignments are ^{1}H/^{15}N-Ser^{70} and ^{1}H/^{15}N-Ala^{237}, whereas for mutant Y105W, the missing assignments are ^{1}H/^{15}N-Ser^{70}, ^{1}H/^{15}N-Asn^{132}, and ^{1}H/^{15}N-Ala^{237}. As observed previously for the E28G assignments (28), the missing chemical shifts are attributed to peaks overlapping or missing resonances caused by line broadening. Regardless of the functional differences resulting from the Y105*X* mutations, the two-dimensional and three-dimensional NMR spectra of all mutants are quite similar to those of the WT enzyme (supplemental Fig. S1). However, depending on the mutation at position 105, important chemical shift differences were observed at specific residues relative to WT. Fig. 1 presents the structural

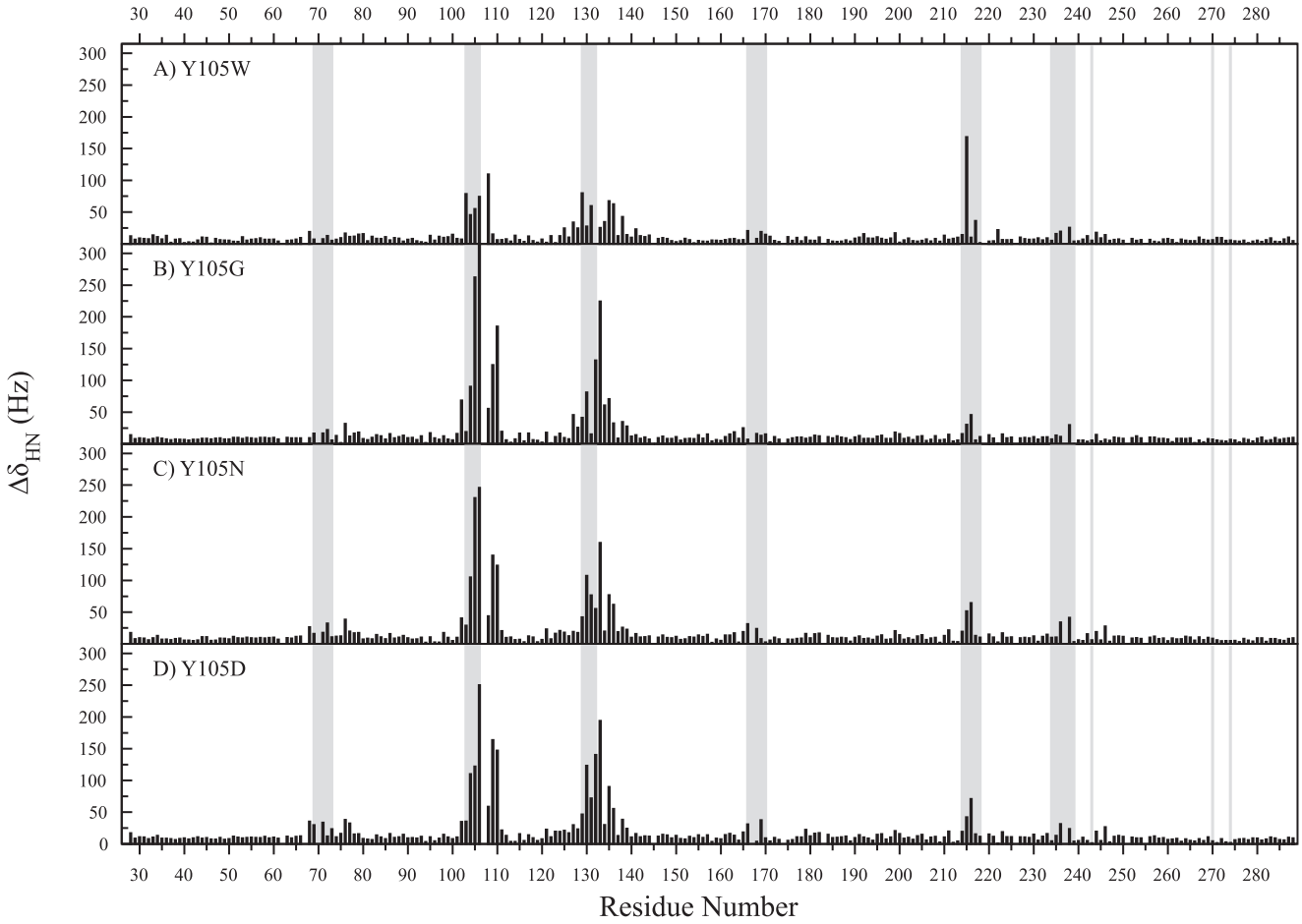

FIGURE 2. **Sequence mapping of ^{1}H-^{15}N backbone chemical shift differences ($\Delta\delta_{HN}$) (Hz) calculated between wild-type TEM-1 and mutants Y105W, Y105G, Y105N, and Y105D.** Residues that define active-site walls of TEM-1 are highlighted in *gray* (see Fig. 3).

mapping of backbone amide chemical shift differences ($\Delta\delta_{HN}$) observed between WT and mutants Y105*X*, whereas Fig. 2 presents the magnitude of these $\Delta\delta_{HN}$ displayed on the primary sequence of the enzyme. For all mutants, the most important effects observed on $\Delta\delta_{HN}$ occur in three major areas of the enzyme corresponding to residues 100–115, 120–140, and 213–218 (Fig. 2). To a lesser extent, all mutants also display higher-than-background effects on $\Delta\delta_{HN}$ in regions encompassing residues 68–80, 163–170, and 235–246. Finally, with the exception of residue 215, $\Delta\delta_{HN}$ is generally smaller for mutant Y105W than for the three other Y105*X* mutants investigated.

Residues in contact with substrate molecules or directly implicated in catalysis in TEM-1 β-lactamase are all located within active-site walls encompassing residues Met^{69}–Lys^{73}, Val^{103}–Ser^{106}, Met^{129}–Asn^{132}, Glu^{166}–Asn^{170}, Val^{214}–Gly^{218}, Lys^{234}–Glu^{239} (Ambler Lys^{234}–Glu^{240}), Arg^{243} (Ambler Arg^{244}), Met^{270} (Ambler Met^{272}), and Asn^{274} (Ambler Asn^{276}) (Fig. 3 and *gray regions* in Figs. 2 and 5). Because these residues are generally located in the immediate vicinity of the substrate molecule and, in some cases, are very close to the mutated residue, some $\Delta\delta_{HN}$ may be the result of a direct short range interaction with residues in close proximity to the Tyr^{105} mutation. For instance, the shortest distance between Tyr^{105} and Asn^{132} (O_{105}–N_{132}) is only 3.0 Å in the crystal structure of the free enzyme (PDB coordinates 1BTL), therefore providing an explanation for the magnitude of $\Delta\delta_{HN}$ observed at position Asn^{132} in all Y105*X* mutants. In contrast, although they form the sub-

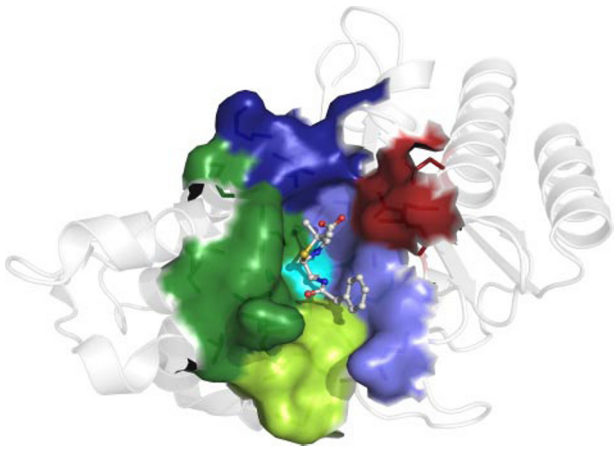

FIGURE 3. **Solvent-accessible surface representation of the active-site walls in TEM-1 β-lactamase.** Residues forming the active-site cavity and either implicated in substrate recognition or catalysis are grouped as follows: Met^{69}–Lys^{73} (*cyan*), Val^{103}–Ser^{106} + Met^{129}–Asn^{132} (SDN loop) (*dark green*), Glu^{166}–Asn^{170} (Ω-loop) (*light green*), Val^{214}–Gly^{218} (*dark blue*), Lys^{234}–Glu^{239} (Ambler Lys^{234}–Glu^{240}) (*light blue*), Arg^{243} (Ambler Arg^{244}) + Met^{270} (Ambler Met^{272}) + Asn^{274} (Ambler Asn^{276}) (*dark red*). The acylated benzylpenicillin substrate is displayed as *balls* and *sticks* (PDB coordinates 1FQG). Residue numbering according to Ambler *et al.* (48).

strate cavity in TEM-1, some of these active-site walls are constituted by residues separated by large distances (*e.g.* the shortest distance between Tyr^{105} and Glu^{166}, O_{105}–O$\epsilon 1_{166}$ = 7.6 Å). Interestingly, the active-site walls are generally more affected by the Y105*X* mutation than any other portion in the enzyme, and most segments of each wall contain at least one residue displaying higher-than-average $\Delta\delta_{HN}$ (Fig. 2). Moreover, whereas being generally concentrated near the active-site cavity, significant effects on $\Delta\delta_{HN}$ are nevertheless observed throughout the enzyme for all mutants, sometimes more than 20 Å from the site of mutation (Fig. 1). This result illustrates that the effect of mutations at position 105 is not restricted to a local environment. In fact, although 57 residues of mutant Y105W display backbone $\Delta\delta_{HN}$ greater than 11 Hz when compared with WT (22% of the total enzyme), this number jumps to 78 residues (30%) in Y105G, 91 residues (35%) in Y105N, and 104 residues (40%) in Y105D (Table 1), thus clearly extending beyond the immediate environment of position 105. In fact, the Y105*X* mutation is too far away from several residues displaying significant $\Delta\delta_{HN}$ to result in any direct contribution to chemical shift changes (*e.g.* backbone $^{15}N_{105}$–$^{15}N_x$ distances = 12.7 Å for Gly^{238}, 12.9 Å for Leu^{169}, and 19.0 Å for Leu^{76}), therefore suggesting the existence of coupled long range effects caused by the mutation at position 105.

TABLE 1
Distribution of ^{1}H-^{15}N backbone chemical shift differences ($\Delta\delta_{HN}$) for residues affected by the Y105*X* mutation

$\Delta\delta_{HN}$ (Hz)[a]	Y105W	Y105G	Y105N	Y105D
	no. of affected residues			
11–20	35	54	59	66
20–30	8	5	11	12
30–40	3	4	4	11
40–50	2	3	4	2
50–60	2	1	2	2
60–70	2	2	2	0
70–80	3	1	2	2
80–90	0	1	0	1
90–100	0	1	0	0
100–125	1	1	3	3
125–150	0	1	1	2
150–200	1	1	1	2
>200	0	3	2	1
Total no. of affected residues	**57 (22%)**	**78 (30%)**	**91 (35%)**	**104 (40%)**
k_{cat} relative to WT[b]	0.73	0.97	1.30	0.21
K_m relative to WT[b]	0.53	3.53	6.42	8.58
k_{cat}/K_m relative to WT[b]	**1.34**	**0.27**	**0.20**	**0.02**

[a] Experimental error = 5.5 Hz. Only values greater than twice the experimental error were considered as significant.
[b] Values for benzylpenicillin, taken from Ref. 25 . WT TEM-1 values: $k_{cat} = 1240\ s^{-1}$; $K_m = 43\ \mu M$; $k_{cat}/K_m = 2.9 \times 10^7\ M^{-1}\ s^{-1}$.

The π-system of aromatic residues such as tyrosine can generate a local magnetic field known as ring current, which may significantly affect the chemical shift of surrounding nuclei. To verify whether short and long range chemical shift differences observed in the Y105*X* mutants could simply be attributed to the disappearance of the aromatic hydroxyphenyl side chain of Tyr^{105}, we used the program SHIFTS (45) to predict ring current effects originating from Tyr^{105}. Ring current shifts were calculated for both previously observed conformations of the Tyr^{105} side chain in crystal structures of TEM-1 (46, 47). Significant ring current shifts for Tyr^{105} were predicted in the immediate vicinity of position 105 (90 Hz predicted for backbone ^1H_N of residue 106, 72 Hz for 108, and less than 36 Hz for residues 109, 110, and 130–132), but no other significant effect (>15 Hz) was predicted for either of the two side chain conformations of residue 105 (results not shown). This indicates that significant long range chemical shift differences observed in all Y105*X* mutants are not attributed to direct electronic perturbation caused by the elimination of the hydroxyphenyl side chain of Tyr^{105}, and therefore must rely on a combination of concerted effects that have consequences throughout the enzyme.

It is also interesting to note that the number and magnitude of the effects on $\Delta\delta_{HN}$ generally correlate with the previously reported catalytic efficiencies of the same mutants for the classical substrate benzylpenicillin (Table 1) (25), suggesting that electronic perturbations and/or dynamic effects observed by NMR may adequately reflect catalytic effects caused by this mutation in TEM-1. Thus, mutant Y105W displays fewer affected residues (22%), consistent with its high catalytic efficiency, whereas 40% of the residues of the weakly active Y105D mutant show significant ^{1}H-^{15}N chemical shift perturbation. This mutant also displays chemical shift perturbation for a greater number of catalytic residues than the other Y105*X* mutants, consistent with its low catalytic efficiency (Y105D-$k_{cat} = 255\ s^{-1}$, Y105D-$K_m = 369\ \mu M$, Y105D-$k_{cat}/K_m = 6.9 \times 10^5\ M^{-1}\ s^{-1}$ *versus* WT-$k_{cat} = 1240\ s^{-1}$, WT-$K_m = 43\ \mu M$, WT-$k_{cat}/K_m = 2.9 \times 10^7\ M^{-1}\ s^{-1}$) (Table 2) (25). In addition, these $\Delta\delta_{HN}$ are generally of greater magnitude as catalytic efficiency decreases.

^{15}N Backbone Relaxation Dynamics—Previous experimental observations made by x-ray crystallography on TEM-1 have shown that Tyr^{105} can adopt two alternate conformations in the presence of substrates or inhibitors (47). Although the Tyr^{105} hydroxyphenyl side chain points toward Val^{216} in the free enzyme, a $\chi 1$ angle rotation of more than 110° has been

TABLE 2
Backbone ^{1}H-^{15}N chemical shift differences ($\Delta\delta_{HN}$) between Y105*X* mutants and wild-type TEM-1 for selected active-site residues

Mutant	$\Delta\delta_{HN}$ (Hz)						k_{cat}/K_m relative to wild type[b]
	Lys^{73} (15.5 Å)[a]	Ser^{130} (10.2 Å)	Asn^{132} (6.1 Å)	Glu^{166} (11.0 Å)	Lys^{234} (18.7 Å)	Arg^{244} (17.3 Å)	
Y105W	NS[c]	**27.4**[d]	NA[e]	**20.2**	NS	NS	1.34
Y105G	5.7	**81.0**	**131.5**	6.8	7.2	5.6	0.27
Y105N	10.6	**107.4**	**55.2**	**31.3**	9.7	5.7	0.20
Y105D	**23.4**	**123.2**	**140.4**	**30.8**	NS	NS	0.02

[a] Distance between backbone $^{15}N_{105}$-$^{15}N_x$ atoms (PDB coordinates 1BTL).
[b] Values for benzylpenicillin were taken from Ref. 25.
[c] NS means not significant.
[d] $\Delta\delta_{HN}$ > 20 Hz are shown in boldface type.
[e] NA means not available.

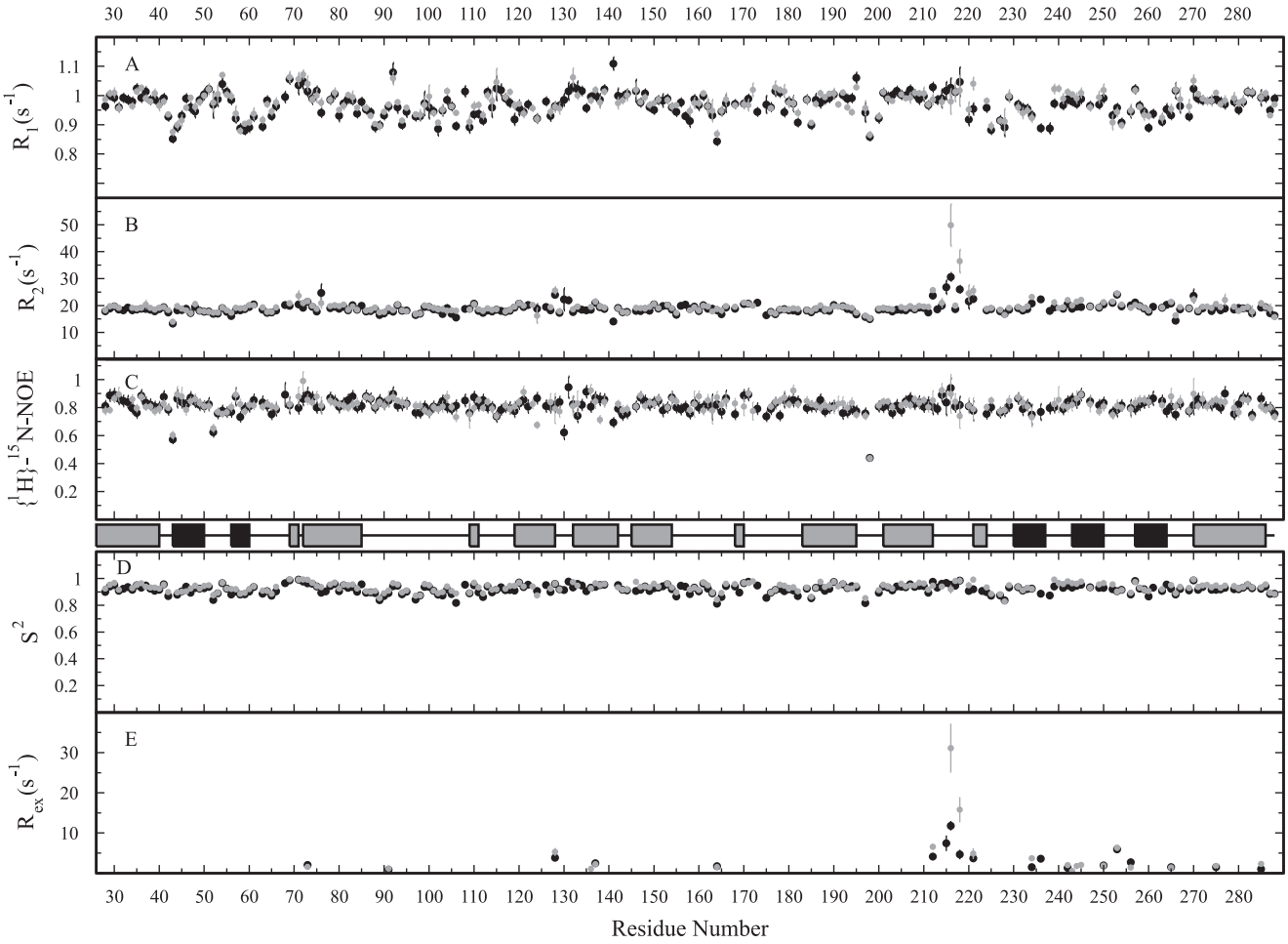

FIGURE 4. **R_1, R_2, and {^{1}H}-^{15}N NOE relaxation parameters and the model-free-calculated parameters S^2 and R_{ex} plotted on the sequence of TEM-1 β-lactamase.** Values for WT are colored *gray*, and values for mutant Y105D are colored *black*. Secondary structure elements are plotted on the sequence as *gray rectangles* for α-helices and *black rectangles* for β-strands.

observed in the presence of the inhibitor imipenem (47), making this the largest conformational change observed in the enzyme. High flexibility of Tyr^{105} is suggested by high *B*-factor values of Tyr^{105} in several crystal structures of TEM-1 (46, 49) and confirmed by a lower-than-average order parameter of this amide in solution as evaluated by NMR (29). However, our previous dynamic modeling studies of this residue showed a low propensity of Tyr^{105} for conformational change on the ps time scale relative to more flexible Y105*X* replacements, suggesting that positioning and restricted dynamic motions of the Tyr^{105} side chain could be a determinant of recognition for substrate stabilization in TEM-1 β-lactamase (25).

TEM-1 Y105D displayed the most important effects on $\Delta\delta_{HN}$ relative to WT as well as a reduction of 2 orders of magnitude in its catalytic efficiency for benzylpenicillin (25). We therefore conducted ^{15}N backbone relaxation dynamics studies to evaluate the importance of local and global dynamic effects caused by the Y105D mutation. To obtain dynamic information on time scales of ps-ns and μs-ms, both longitudinal (R_1) and transverse (R_2) ^{15}N relaxation rates as well as {^{1}H}-^{15}N NOE values were measured and are presented in Fig. 4 for both WT and mutant Y105D (raw data presented in supplemental material). We observed a significant variation of relaxation data and global tumbling times as a function of protein concentration. For example, the global correlation time for TEM-1 varied from 12.8 ns at 0.4 mM to 13.8 ns at 0.8 mM. This increase in correlation time is most likely due to an increase in viscosity at high protein concentration. It was therefore crucial for our analysis that both proteins be at exactly the same concentration. From the ^{1}H-^{15}N HSQC spectra recorded for the relaxation experiments, it was possible to obtain reliable data for 206 and 230 out of 250 potentially observable amides for WT and mutant Y105D, respectively. Table 3 presents average values for relaxation data and parameters obtained for TEM-1 and mutant Y105D.

TABLE 3
Average backbone relaxation and model-free parameters for wild-type TEM-1 and mutant Y105D

	TEM-1	Y105D
R_1	0.98 ± 0.01	0.97 ± 0.02
R_2	19.5 ± 0.6	18.8 ± 0.7
NOE	0.82 ± 0.04	0.81 ± 0.04
S^2	0.93 ± 0.02	0.92 ± 0.02
$D_\parallel/D_\perp$	1.16 ± 0.01	1.18 ± 0.01
τ_m (ns)	13.8 ± 0.01	13.7 ± 0.01

The general comparison of R_1, R_2, and {^{1}H}-^{15}N NOE values for TEM-1 and mutant Y105D shows that both enzymes behave in a very similar manner, displaying comparable values throughout the sequence (Table 3 and Fig. 4, *A*–*C*). The general

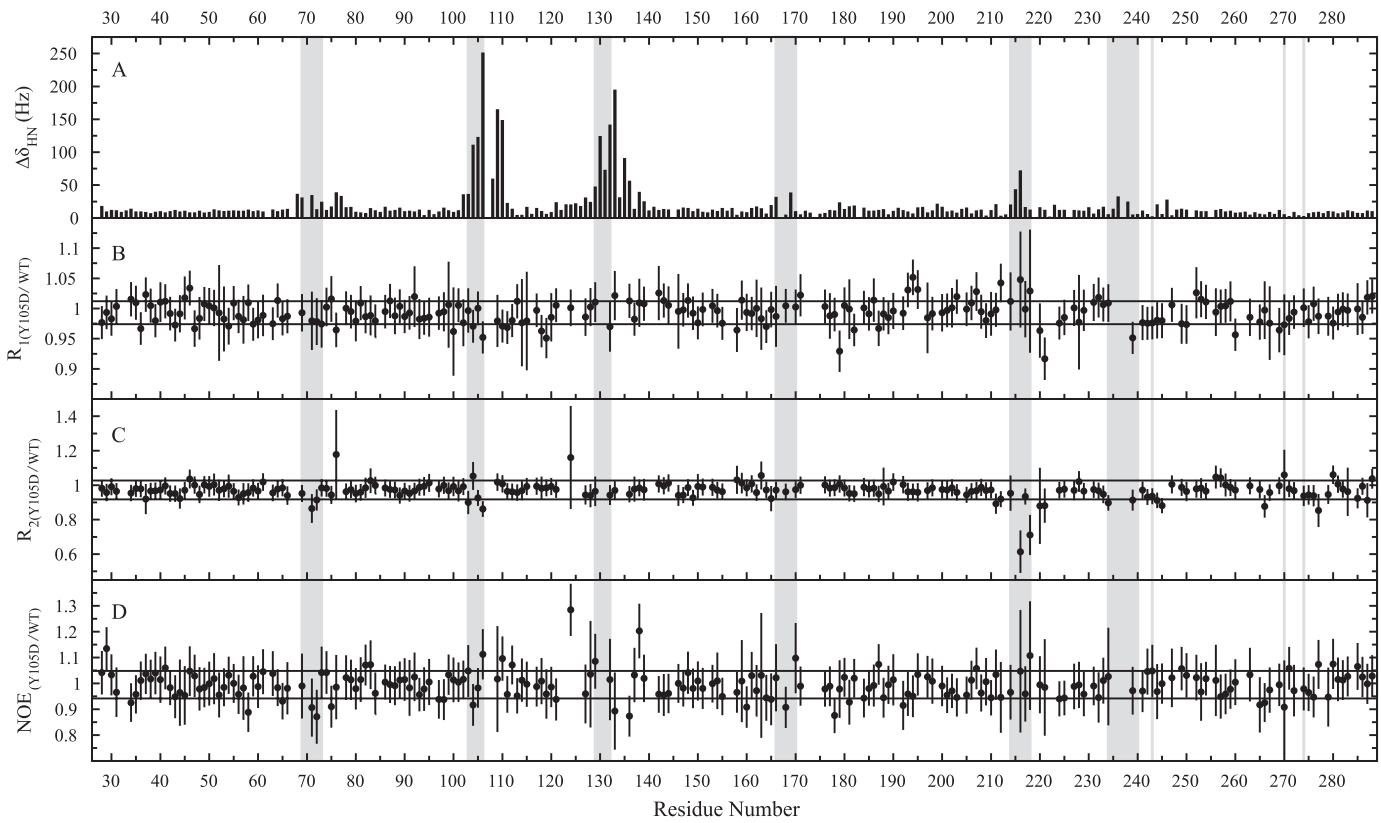

FIGURE 5. **Y105D/WT ratios for the relaxation parameters (R_1, R_2, and {^{1}H}-^{15}N NOE).** *A* displays $\Delta\delta_{HN}$ (Hz) calculated for mutant Y105D. *B*, *C*, and *D* display Y105D/WT ratios for R_1, R_2 and NOE parameters, respectively. Means ± S.D. are represented as a *rectangle* for each ratio. Values outside of the standard deviation areas were considered as significant.

TABLE 4

Active-site wall and invariant residues displaying significant relaxation parameter variation between wild-type TEM-1 and mutant Y105D

Variations in R_1, R_2, and NOE were considered significant if the Y105D/WT ratio was larger than the average ratio $\pm 1\sigma$. Variations in S^2 were considered significant if the difference was larger than the sum of the errors + 0.01. Variations in R_{ex} were considered significant if the difference was larger than the sum of the errors + 1.0 s^{-1}.

Relaxation parameter	Residues[a]
R_1	Tyr^{46}, Leu^{76}, **Glu^{104}**, **Ser^{106}**, **Asn^{132}**, Arg^{164}, **Val^{216}**, **Gly^{218}**, Leu^{220}, Ala^{232}, **Glu^{239}**, Gly^{250}, **Met^{270}**, Trp^{288}
R_2	Tyr^{46}, **Thr^{71}**, **Phe^{72}**, Leu^{76}, **Val^{103}**, **Glu^{104}**, **Ser^{106}**, **Lys^{215}**,[b] **Val^{216}**, **Gly^{218}**, Leu^{220}, **Lys^{234}**, **Glu^{239}**, Gly^{244}, **Met^{270}**, Ile^{280}, Trp^{288}
{^{1}H}-^{15}N NOE	**Thr^{71}**, **Phe^{72}**, **Val^{103}**, **Glu^{104}**, **Ser^{106}**, **Met^{129}**, **Glu^{168}**, **Asn^{170}**, Thr^{181}, **Gly^{218}**, **Arg^{243}**, Leu^{249}, **Met^{270}**, Ile^{280}
S^2	**Ser^{106}**, **Glu^{239}**
R_{ex}	**Lys^{215}**, **Val^{216}**, **Gly^{218}**, **Lys^{234}**

[a] Residues defining active-site walls are in boldface type and residues intolerant to any amino acid substitution in TEM-1 (55) are underlined. Sequential numbering is used.
[b] As the ^{15}N-HSQC correlation of Lys^{215} was significantly weaker for the WT than for Y105D, it was impossible to obtain relaxation data for the WT. We therefore conclude that the R_2 value was significantly higher for the WT, reflecting significantly higher R_{ex}.

constant pattern observed in the relaxation data from one extremity of the enzyme to the other is uncommon relative to the pattern generally observed in other proteins, where an important decrease in both N- and C-terminal regions as well as in unstructured regions is frequently observed. This feature reflects the high rigidity of both enzymes in solution, a property that we have also previously observed in TEM-1 (E28G) (29). However, there are significant local differences between the relaxation data for both enzymes, especially concentrated in regions showing important chemical shift differences (*e.g.* residues 70–80, 124–135, and most importantly 211–221) (Fig. 4, *A–C*). Fig. 5 shows the Y105D/WT ratios for all relaxation parameters, highlighting the residues displaying the most important differences between both enzymes. Changes in R_1 and {^{1}H}-^{15}N NOE values reflect differences in the ps-ns dynamics of proteins, whereas changes in R_2 values may also reflect changes in μs-ms motions. Interestingly, 88 residues are significantly affected in either R_1 or {^{1}H}-^{15}N NOE relaxation parameters, suggesting significant dynamic differences on the ps-ns time scale for these residues (supplemental Table S3). Among these, 14 belong to the active-site walls of TEM-1 and may be implicated in substrate stabilization (Table 4). Because it has been proposed that motions on the ps-ns time scale may influence the thermodynamics of binding as well as the kinetics of enzyme-catalyzed reactions (50–52), disruption of ps-ns motions among these active-site residues may reduce substrate stabilization and/or catalysis in mutant Y105D. Similarly, among the 30 residues significantly affected in R_2 (supplemental Table S3), 11 belong to the active-site walls (Table 4), suggesting that differences in μs-ms motions of these residues between WT and mutant Y105D may also affect substrate stabilization and/or catalysis. Residues 211–221 correspond to the region where the R_2 values are the most affected by the Y105D mutations, both in terms of magnitude and number of residues

affected. In addition, because μs-ms dynamics are directly related to the time scale of catalysis, these modified motions may also affect turnover in mutant Y105D. Residue Lys^{234} is also a particularly good candidate for this, as it has been shown to be an essential member of the catalytically important hydrogen-bonding sub-network of class A β-lactamases through the formation of a hydrogen bond with Ser^{130} (an equally important member of the SDN loop implicated in catalysis) (53).

Model-free Analysis—To correlate our relaxation data with the internal dynamics of the protein, further dynamic analyses were conducted using the model-free formalism pioneered by Lipari and Szabo (39, 40). Such analyses allow for the direct investigation of local and global dynamic effects observed in the protein of interest, namely through the extraction of the order parameter (S^2), the conformational exchange parameter (R_{ex}), and the overall correlation time of the molecule (τ_m) (Tables 3 and 4 and Fig. 4, *D* and *E*).

Average values of model-free parameters for WT and mutant Y105D confirm that both enzymes behave very similarly with respect to their global dynamic properties (Table 3). Following the model selection, there was only a slight divergence between both proteins; for WT and mutant Y105D, respectively, 82 and 81% of the residues fitted well for model 1, 7 and 9% for model 2, and 10 and 8% for model 3. No residue was fitted to model 4 nor model 5 in either protein. Both WT and Y105D display a small prolate axial anisotropy with $D_{\parallel}/D_{\perp}$ values of 1.16 and 1.18 and similar global correlation times (τ_m) of 13.8 and 13.7 ns, respectively (Table 3). Considering that the two enzymes differ only by a single mutation, this result was expected. In addition, the average order parameter values (S^2) obtained for TEM-1 and mutant Y105D are exceptionally high (>0.9 for both enzymes), confirming previous observations reported for TEM-1 (E28G) (29). Because the order parameter measures the amplitude of ps-ns motions and varies from 0 for unrestricted internal motions to 1 for completely restricted motions (43), values >0.9 are indicative of highly ordered proteins in solution.

Six residues display distinct behavior patterns in their order parameters (S^2) (supplemental Table S3), two of which are located in the active-site walls (Ser^{106} and Glu^{239}) (Table 4). These residues display a significant decrease in their order parameters indicating an increase in ps-ns motion amplitude in the mutant compared with WT. Furthermore, five residues display distinct μs-ms motions when compared with WT (supplemental Table S3), four of which belong to active-site walls (Lys^{215}, Val^{216}, Gly^{218}, and Lys^{234}) (Table 4). The model-free analysis for these residues required an R_{ex} term, which is related to local conformational exchange and refers to motions observed on the μs-ms time scale (43). As the ^{15}N-HSQC correlation of residue Lys^{215} was significantly weaker for the WT than for Y105D, it was impossible to obtain relaxation data for this residue in the WT. We therefore conclude that the R_2 value was significantly higher for the WT, reflecting significantly higher R_{ex} for Lys^{215} in the WT. The important decrease of R_2 and R_{ex} for residues 215, 216, 218, and 234 in mutant Y105D (Fig. 4*E*) suggests a slowdown in motions of these residues on the catalytically relevant μs-ms time scale. These residues delineate two active-site walls of TEM-1, and Lys^{215}, Val^{216}, and Gly^{218} are located in the most dynamically affected region

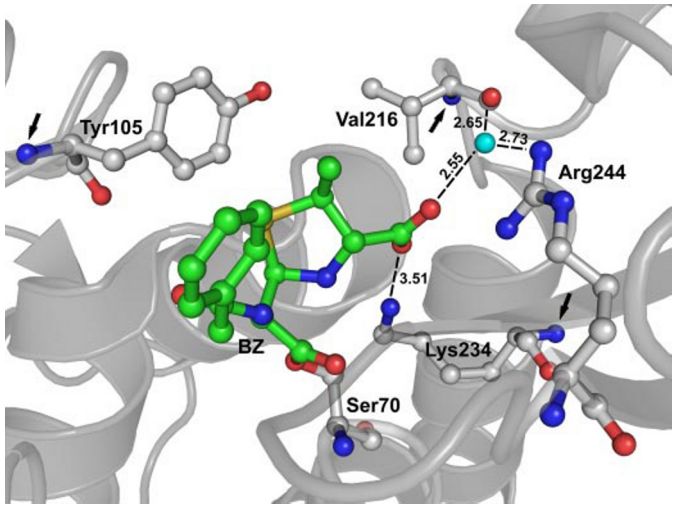

FIGURE 6. **Substrate anchoring at the active site of TEM-1 β-lactamase (PDB coordinates 1FQG).** Conserved water molecule 294 (Wat^{294}, represented as a *cyan ball*) is anchored by the guanidinium moiety of Arg^{244} and the backbone carbonyl of Val^{216} (adapted from Ref. 58). Lys^{234} and Wat^{294} contribute to ligand binding by stabilizing the C3 carboxylate group of the substrate. Backbone ^{15}N atoms of residues Tyr^{105}, Val^{216}, and Lys^{234} are identified by *arrows* (distances in 1BTL: $^{15}N_{105}$ to $^{15}N_{234}$ = 18.7 Å and $^{15}N_{105}$–$^{15}N_{216}$ = 14.7 Å). Residues Ser^{70}, Tyr^{105}, Val^{216}, Lys^{234}, and Arg^{244} and the acylated benzylpenicillin substrate are displayed as *balls* and *sticks*. Ambler numbering (48) is used and all distances are expressed in Å.

observed between WT and mutant Y105D (Fig. 4). It is interesting that for this region (211–221), only two residues exhibit small but significant chemical shift differences (Lys^{215} and Val^{216}), although changes in motional parameters occur for a greater number of residues and are more important, as reflected in the fact that this region displays the most significant changes in R_2 and R_{ex} values. Assuming exchange in a two-state model, this could suggest that for these residues the rate of exchange between the two states is significantly affected by the mutation, but the population of each state is roughly the same in the WT and in mutant Y105D. Therefore, only the rate of exchange would be significantly affected by the mutation.

Despite the fact that the model-free approach is not the most comprehensive evaluation of μs-ms time scale motions, dynamics on this time scale can be inferred from R_2. Crude R_2 values do not necessarily provide an adequate portrayal of μs-ms dynamics for an enzyme, but differences in R_2 for WT and mutant Y105D suggest μs-ms motion differences resulting from this mutation. In addition to the important R_{ex} differences noted for positions 215, 216, 218, and 234, 13 additional active-site wall or invariant residues may have different μs-ms motions between WT and Y105D, based on significant variation in R_2 (Table 4). Motions of Val^{216} and Lys^{234} on a catalytically relevant time scale could affect catalysis by perturbing the hydrogen bonding network observed in WT (Fig. 6), therefore partly explaining the differences in k_{cat} observed previously with mutant Y105D (25).

DISCUSSION

The investigation of the correlations between enzyme dynamics and function is required to gain a detailed understanding of the mechanisms underlying the catalytic activity of these important molecules. Implication of ps-ns and μs-ms

motions in enzyme activities and catalytic rates is now well accepted, and NMR spectroscopy is a valuable tool to probe these time windows (21). In an attempt to explain the differences in the catalytic efficiency of several Y105*X* mutants of TEM-1, we previously conducted a short 200-ps molecular dynamics simulation that allowed for the partial explanation of differences in affinity through the formation of a stabilizing wall created by residues exhibiting few degrees of freedom at position 105, therefore restricting substrate motion in the active site (25). However, this molecular dynamics simulation model was relatively limited in that it only allowed for the investigation of small motions explored on a short time scale and exclusively concentrated in the local environment of position 105. To better characterize these motions, we investigated the role of the conserved active-site residue Tyr^{105} by comparing its structural and dynamic features with respect to the Y105W, Y105G, Y105N, and Y105D mutants using NMR spectroscopy. The chemical shift differences observed between TEM-1 and these various mutants allowed us to focus our dynamic characterization on the Y105D mutant.

Overall, although the Y105D mutation considerably affects the electronic and dynamic environment of several residues throughout the enzyme, the backbone dynamics of residue 105 are not significantly affected relative to WT, suggesting that local dynamics at position 105 are not the sole element contributing to the differences observed in catalysis. Indeed, despite the important steric and ionic alterations offered by the Y105D replacement, R_1, R_2, and $\{^1H\}$-^{15}N NOE values of mutant Y105D remain similar to WT. On the other hand, our present analyses revealed significant short and long range changes in motion throughout the enzyme, providing further clarification of the effect of this mutation in substrate stabilization and catalysis. We show significant alterations in the ps-ns and μs-ms dynamics of important residues, often either in or near the active-site walls of TEM-1, as a result of this mutation at position 105. For instance, Ser^{106} and Glu^{239} show significant increase in ps-ns motions with respect to WT. Such a decrease of the order parameter for residues located in the active site could result in a higher conformational entropy cost associated with substrate binding, hence contributing to the catalytically impaired active-site observed in the Y105D mutant. In addition, Arg^{164} is a highly conserved residue in class A β-lactamases that is considered to be important in anchoring the base of the Ω-loop through a salt bridge with Asp^{179} (54). Although more than 17 Å away from the mutation at position 105, a significant change in the R_1 is observed. This change in ps-ns dynamics through a possible network of active-site motions could affect the stability of the Ω-loop and thus reduce appropriate substrate stabilization and catalysis.

Moreover, our results show a significant decrease in the μs-ms motions for residues Glu^{212}, Lys^{215}, Val^{216}, Gly^{218}, and Lys^{234}. It is interesting to note that among these residues, Val^{216} and Lys^{234} were shown to be intolerant to any amino acid substitutions with respect to benzylpenicillin hydrolysis in TEM-1 (55). These results suggest that this activity requirement may partly be governed by μs-ms dynamics in the vicinity of these residues. Lys^{215}, Val^{216}, and Lys^{234} are positioned in the immediate vicinity of the substrate molecule, and their ground-state dynamic behavior may have a direct impact on substrate recognition and stabilization, therefore partly explaining the decreased affinity observed for mutant Y105D (25). In fact, although Lys^{234} is implicated in the initial recognition of the substrate molecule as an electrostatic anchor for the carboxylate moiety of substrates (56), its implication in proton shuttling during catalysis is still the subject of debate (57). On the other hand, with help from the guanidinium group of Arg^{244}, the backbone carbonyl group of Val^{216} has been shown to anchor a conserved water molecule that interacts with the C3 carboxylate group of the substrate for appropriate stabilization (58) (Fig. 6). Thus, this residue has been suggested to influence substrate binding and catalysis in both TEM-1 (55) and PSE-4 (59). Because the μs-ms motions surrounding Glu^{212}, Lys^{215}, Val^{216}, and Lys^{234} are decreased in mutant Y105D, these changes on the catalytically relevant time scale of their local environment may reduce substrate stabilization in the active site of Y105D, consistent with the large increase in K_m previously observed with this mutant (25). In addition to affecting the correct stabilization of the substrate through a conserved water molecule by Val^{216} (Fig. 6), the attenuation of μs-ms motions in the Y105D mutant could reflect a reduction of the possible conformations that the enzyme can adopt on this time scale. These "productive" conformations could be responsible for the appropriate positioning of the substrate in the active site, and their loss upon mutation could account for the decline of the enzymatic activity. It should be noted that the present study confirmed the presence as well as the importance of previously observed μs-ms motions in the active site and in the Ω-loop of TEM-1 (29). Although it was observed that μs-ms motions were present in the vicinity of the active site (29), it was impossible to determine whether these motions were catalytically relevant. The changes in μs-ms time scale motions we observe upon a mutation that affects kinetic properties of TEM-1 indicates a correlation between motion time scales and the kinetic properties, consistent with causality, although causality has not been demonstrated. To date, the numerous x-ray studies of TEM-1 have provided no indication of catalytically related motions. As a result of the current NMR studies, we propose that the combination of these subtle but significant effects within the active-site cavity are directly related to the 2 orders of magnitude reduction in catalytic efficiency observed for the Y105D mutant of TEM-1 (25). It is important to note that the available data do not allow us to differentiate whether the μs-ms motions observed for the amides of Glu^{212}, Lys^{215}, Val^{216}, Gly^{218}, and Lys^{234} are resulting from their own motions or from motions of other surrounding residues. However, it is now clear that these μs-ms motions are correlated with the fine-tuning of catalytic properties of TEM-1, and possibly of other β-lactamases.

Long Range Dynamic Effects—Although important residues displaying modified ps-ns and μs-ms dynamics in mutant Y105D are elements of the active-site walls and therefore generally considered in close proximity to the substrate molecule, it is important to keep in mind that motions characterized in this study are exclusively focused on the backbone relaxation of ^{15}N atoms. To that extent, it is important to estimate relevant distances separating residues of interest and therefore to clarify what is considered short range ($<$5 Å) or long range ($>$5 Å)

interactions. For instance, the shortest distance between Tyr^{105} and Val^{216} (OH_{105}–$C\gamma1_{216}$ = 4.2 Å) may be considered short range, whereas the distance between both their ^{15}N atoms would be considered long range (14.7 Å). This important difference in atom distances is observed for several residues located in the active-site walls of TEM-1. Nonetheless, most of the calculated distances among dynamically affected residues should be considered long range because they do not permit any direct contact with residue 105. For instance, Lys^{234} displays a shortest residue distance of 7.8 Å with Tyr^{105} ($C\epsilon2_{105}$–$N\zeta_{234}$) and a $^{15}N_{105}$–$^{15}N_{234}$ distance of 18.7 Å (both long range).

This observation raises two important points regarding dynamic results characterized in this study. The first point is the fact that, except for dynamically affected residues located in the immediate vicinity of the mutation (*e.g.* Ser^{106}, Asn^{132}, and to a certain extent Val^{216}), both shortest inter-residue or NMR observable (backbone ^{15}N atoms) distances between position 105 and any other dynamically affected residue are too important to account for any direct interaction (*e.g.* Lys^{234}, Leu^{76}, Gly^{218}, etc.). This observation raises the second important point: the long range dynamic effects observed as a consequence of the Y105D mutation is consistent with the existence of a network of motions among residues of TEM-1 β-lactamase. This hypothesis is strengthened by a previous molecular dynamics study performed on the inhibitor-resistant M69L mutant of TEM-1, suggesting that only differences in dynamics of this mutant account for the resistance to clavulanate (30). This type of dynamic network explaining long range dynamic effects has been characterized previously in detail for other enzymes and has often been shown to play a crucial role in catalysis (reviewed in Refs. 23 and 24). It has also been observed in allosteric (60) and other noncatalytic proteins (61) with long range motions characterized as contiguous (displaying a traceable pathway) or disperse (noncontiguous with an untraceable pathway). The evidence presented here not only suggests dynamic "cross-talk" between residues constituting opposite walls of the active-site cavity of TEM-1 (often separated by large distances) but also suggests that residues distal to the active-site cavity may disrupt catalysis in TEM-1 through their altered motional behavior. For instance, it is interesting to note that several residues displaying significant ps-ns and/or μs-ms motional differences have been shown to be intolerant to any amino acid substitution in TEM-1 (Table 4), among which several are conserved in all class A β-lactamases (55). Although some residues of the active-site walls are expected to be intolerant to any mutation because of their direct importance in catalysis (*e.g.* Lys^{234} and Val^{216}), others are distal to the active-site cavity and display significant dynamic alterations between TEM-1 and mutant Y105D. For example, two dynamically affected residues (Tyr^{46} and Leu^{76}, both >20 Å from the mutation) are completely buried in TEM-1, and their motional disruption through a possible long range network of coupled motions may affect the appropriate packing of the hydrophobic core of the enzyme and/or catalysis.

The fact that our NMR studies on WT and mutants Y105*X* were performed in the absence of any substrate or inhibitor is of considerable interest because it supports previous investigations showing that catalytically relevant motions are often observed in the free enzyme (10, 20). The conservation of motions in absence of substrate may be an essential component of enzyme evolution and may contribute to explain the exceptionally high acceleration rates observed in enzyme catalysis. In addition, as previously pointed out (23), this finding may have interesting implications for the understanding of the secondary and tertiary elements conserved in several protein folds. Assuming that the conserved fold observed for all class A β-lactamases is partly governed by an evolutionary constraint preserving elements that define dynamic motions essential to their catalytic function, the characterization of such elements would greatly advance our understanding of class A β-lactamase catalysis as well as their importance in antibiotic resistance. A common structural organization of functionally relevant regions that undergo similar concerted movements was recently revealed in the protease enzymatic superfamily (62). Whether the presence of such a network of motions is relevant to the class A β-lactamase fold and similar catalytic mechanisms is beyond the scope of this study. Nevertheless, considering the long range dynamic effects characterized here, it is reasonable to assume that dynamic differences between TEM-1 and various mutants are involved in the observed differences in activity.

Acknowledgment—Equipment was purchased with grants (to S. M. G.) from the Canada Foundation for Innovation.

REFERENCES

1. Neet, K. E. (1998) *J. Biol. Chem.* **273,** 25527–25528
2. Garcia-Viloca, M., Gao, J., Karplus, M., and Truhlar, D. G. (2004) *Science* **303,** 186–195
3. Benkovic, S. J., and Hammes-Schiffer, S. (2003) *Science* **301,** 1196–1202
4. Hammes-Schiffer, S. (2002) *Biochemistry* **41,** 13335–13343
5. Epstein, D. M., Benkovic, S. J., and Wright, P. E. (1995) *Biochemistry* **34,** 11037–11048
6. Osborne, M. J., Schnell, J., Benkovic, S. J., Dyson, H. J., and Wright, P. E. (2001) *Biochemistry* **40,** 9846–9859
7. Agarwal, P. K., Billeter, S. R., Rajagopalan, P. T., Benkovic, S. J., and Hammes-Schiffer, S. (2002) *Proc. Natl. Acad. Sci. U. S. A.* **99,** 2794–2799
8. Radkiewicz, J. L., and Brooks, C. L. (2000) *J. Am. Chem. Soc.* **122,** 225–231
9. Agarwal, P. K., Geist, A., and Gorin, A. (2004) *Biochemistry* **43,** 10605–10618
10. Eisenmesser, E. Z., Millet, O., Labeikovsky, W., Korzhnev, D. M., Wolf-Watz, M., Bosco, D. A., Skalicky, J. J., Kay, L. E., and Kern, D. (2005) *Nature* **438,** 117–121
11. Agarwal, P. K., Webb, S. P., and Hammes-Schiffer, S. (2000) *J. Am. Chem. Soc.* **122,** 4803–4812
12. Bahnson, B. J., Colby, T. D., Chin, J. K., Goldstein, B. M., and Klinman, J. P. (1997) *Proc. Natl. Acad. Sci. U. S. A.* **94,** 12797–12802
13. Billeter, S. R., Webb, S. P., Agarwal, P. K., Iordanov, T., and Hammes-Schiffer, S. (2001) *J. Am. Chem. Soc.* **123,** 11262–11272
14. Colby, T. D., Bahnson, B. J., Chin, J. K., Klinman, J. P., and Goldstein, B. M. (1998) *Biochemistry* **37,** 9295–9304
15. Derreumaux, P., and Schlick, T. (1998) *Biophys. J.* **74,** 72–81
16. Desamero, R., Rozovsky, S., Zhadin, N., McDermott, A., and Callender, R. (2003) *Biochemistry* **42,** 2941–2951
17. Guallar, V., Jacobson, M., McDermott, A., and Friesner, R. A. (2004) *J. Mol. Biol.* **337,** 227–239
18. Rozovsky, S., Jogl, G., Tong, L., and McDermott, A. E. (2001) *J. Mol. Biol.* **310,** 271–280
19. Rozovsky, S., and McDermott, A. E. (2001) *J. Mol. Biol.* **310,** 259–270
20. Beach, H., Cole, R., Gill, M. L., and Loria, J. P. (2005) *J. Am. Chem. Soc.* **127,**

9167–9176
21. Kovrigin, E. L., and Loria, J. P. (2006) *Biochemistry* **45,** 2636–2647
22. Kovrigin, E. L., and Loria, J. P. (2006) *J. Am. Chem. Soc.* **128,** 7724–7725
23. Agarwal, P. K. (2006) *Microb. Cell. Fact.* **5,** 2
24. Tousignant, A., and Pelletier, J. N. (2004) *Chem. Biol.* **11,** 1037–1042
25. Doucet, N., De Wals, P. Y., and Pelletier, J. N. (2004) *J. Biol. Chem.* **279,** 46295–46303
26. Jarymowycz, V. A., and Stone, M. J. (2006) *Chem. Rev.* **106,** 1624–1671
27. Akke, M. (2002) *Curr. Opin. Struct. Biol.* **12,** 642–647
28. Savard, P. Y., Sosa-Peinado, A., Levesque, R. C., Makinen, M. W., and Gagné, S. M. (2004) *J. Biomol. NMR* **29,** 433–434
29. Savard, P. Y., and Gagné, S. M. (2006) *Biochemistry* **45,** 11414–11424
30. Meroueh, S. O., Roblin, P., Golemi, D., Maveyraud, L., Vakulenko, S. B., Zhang, Y., Samama, J. P., and Mobashery, S. (2002) *J. Am. Chem. Soc.* **124,** 9422–9430
31. Sosa-Peinado, A., Mustafi, D., and Makinen, M. W. (2000) *Protein Expression Purif.* **19,** 235–245
32. Farrow, N. A., Muhandiram, R., Singer, A. U., Pascal, S. M., Kay, C. M., Gish, G., Shoelson, S. E., Pawson, T., Forman-Kay, J. D., and Kay, L. E. (1994) *Biochemistry* **33,** 5984–6003
33. Zhu, G., Xia, Y. L., Nicholson, L. K., and Sze, K. H. (2000) *J. Magn. Reson.* **143,** 423–426
34. Gagné, S. M., Tsuda, S., Spyracopoulos, L., Kay, L. E., and Sykes, B. D. (1998) *J. Mol. Biol.* **278,** 667–686
35. Tjandra, N., Wingfield, P., Stahl, S., and Bax, A. (1996) *J. Biomol. NMR* **8,** 273–284
36. Delaglio, F., Grzesiek, S., Vuister, G. W., Zhu, G., Pfeifer, J., and Bax, A. (1995) *J. Biomol. NMR* **6,** 277–293
37. Johnson, B. A., and Blevins, R. A. (1994) *J. Biomol. NMR* **4,** 603–614
38. Nicholson, L. K., Kay, L. E., Baldisseri, D. M., Arango, J., Young, P. E., Bax, A., and Torchia, D. A. (1992) *Biochemistry* **31,** 5253–5263
39. Lipari, G., and Szabo, A. (1982) *J. Am. Chem. Soc.* **104,** 4559–4570
40. Lipari, G., and Szabo, A. (1982) *J. Am. Chem. Soc.* **104,** 4546–4559
41. Clore, G. M., Driscoll, P. C., Wingfield, P. T., and Gronenborn, A. M. (1990) *Biochemistry* **29,** 7387–7401
42. Clore, G. M., Szabo, A., Bax, A., Kay, L. E., Driscoll, P. C., and Gronenborn, A. M. (1990) *J. Am. Chem. Soc.* **112,** 4989–4991
43. Mandel, A. M., Akke, M., and Palmer, A. G., III (1995) *J. Mol. Biol.* **246,** 144–163
44. Pawley, N. H., Wang, C., Koide, S., and Nicholson, L. K. (2001) *J. Biomol. NMR* **20,** 149–165
45. Xu, X. P., and Case, D. A. (2001) *J. Biomol. NMR* **21,** 321–333
46. Jelsch, C., Mourey, L., Masson, J. M., and Samama, J. P. (1993) *Proteins* **16,** 364–383
47. Maveyraud, L., Mourey, L., Kotra, L. P., Pedelacq, J. D., Guillet, V., Mobashery, S., and Samama, J. P. (1998) *J. Am. Chem. Soc.* **120,** 9748–9752
48. Ambler, R. P., Coulson, A. F., Frère, J. M., Ghuysen, J. M., Joris, B., Forsman, M., Levesque, R. C., Tiraby, G., and Waley, S. G. (1991) *Biochem. J.* **276,** 269–270
49. Strynadka, N. C., Adachi, H., Jensen, S. E., Johns, K., Sielecki, A., Betzel, C., Sutoh, K., and James, M. N. (1992) *Nature* **359,** 700–705
50. Kern, D., and Zuiderweg, E. R. (2003) *Curr. Opin. Struct. Biol.* **13,** 748–757
51. Wand, A. J. (2001) *Nat. Struct. Biol.* **8,** 926–931
52. Wand, A. J. (2001) *Science* **293,** 1395
53. Matagne, A., Lamotte-Brasseur, J., and Frère, J. M. (1998) *Biochem. J.* **330,** 581–598
54. Vakulenko, S. B., Taibi-Tronche, P., Toth, M., Massova, I., Lerner, S. A., and Mobashery, S. (1999) *J. Biol. Chem.* **274,** 23052–23060
55. Huang, W. Z., Petrosino, J., Hirsch, M., Shenkin, P. S., and Palzkill, T. (1996) *J. Mol. Biol.* **258,** 688–703
56. Lenfant, F., Labia, R., and Masson, J. M. (1991) *J. Biol. Chem.* **266,** 17187–17194
57. Meroueh, S. O., Fisher, J. F., Schlegel, H. B., and Mobashery, S. (2005) *J. Am. Chem. Soc.* **127,** 15397–15407
58. Wang, X., Minasov, G., and Shoichet, B. K. (2002) *J. Biol. Chem.* **277,** 32149–32156
59. Sabbagh, Y., Thériault, E., Sanschagrin, F., Voyer, N., Palzkill, T., and Levesque, R. C. (1998) *Antimicrob. Agents Chemother.* **42,** 2319–2325
60. Suel, G. M., Lockless, S. W., Wall, M. A., and Ranganathan, R. (2003) *Nat. Struct. Biol.* **10,** 59–69
61. Clarkson, M. W., Gilmore, S. A., Edgell, M. H., and Lee, A. L. (2006) *Biochemistry* **45,** 7693–7699
62. Carnevale, V., Raugei, S., Micheletti, C., and Carloni, P. (2006) *J. Am. Chem. Soc.* **128,** 9766–9772
63. Quenouille, M. (1949) *J. R. Stat. Soc. Ser. B* **11,** 18–84